On the other hand, if the term inside the square root is negative, then ${c_g}^A$ is complex-valued, meaning that weakly nonlinear effects cause the wavepacket envelope to grow exponentially in time. Such waves are said to be 'modulationally unstable'.

The formula (4.35) is used to give a mathematical definition for modulational stability:

$$\begin{aligned} &\text{modulationally stable waves:} \quad \omega_2 \frac{\partial^2 \omega_0}{\partial k^2} > 0 \\ &\text{modulationally unstable waves:} \quad \omega_2 \frac{\partial^2 \omega_0}{\partial k^2} < 0. \end{aligned} \tag{4.36}$$

The criterion depends upon the rate of change with the wavenumber of the group velocity predicted by linear theory and upon the order-amplitude-squared correction to the dispersion relation.

Modulational instability does not imply wave breaking. It means only that weakly nonlinear effects act initially within a wavepacket to increase the maximum value of its amplitude envelope. The consequent evolution depends upon the fully nonlinear dynamics of the waves in question. For example, depending upon the dispersion relation and the initial wave amplitude, finite-amplitude waves can transfer energy back and forth between different frequencies, through what is known as the 'Fermi–Pasta–Ulam' recurrence phenomenon or, for deep water waves in particular, 'Benjamin–Feir' instability.

4.3 Weakly nonlinear interfacial waves

In Section 2.3.2 we examined the structure and dispersion relation associated with small-amplitude waves at the interface of a two-layer fluid with infinitely deep upper and lower layers. Here we will apply the general approach outlined above to examine how the structure and dispersion relation is modified when the wave amplitude is not negligibly small.

4.3.1 Theory for interfacial waves in infinitely deep fluid

As in Section 2.3.2, we suppose the background density profile is given by

$$\bar{\rho}(z) = \begin{cases} \rho_1 & z \geq 0 \\ \rho_2 & z < 0, \end{cases} \tag{4.37}$$

and we let φ and ϕ represent the velocity potentials in the upper and lower layers, respectively, as shown in Figure 4.1. The vertical displacement of the interface is represented by η.

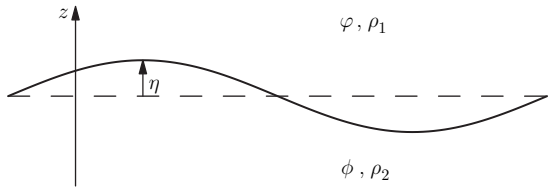

Fig. 4.1. Schematic illustrating the displacement η of the interface between two infinitely deep layers of fluid. The upper fluid has density ρ_1 with a velocity potential ϕ_1, and the lower fluid has density ρ_2 with a velocity potential ϕ_2.

The motion within each layer due to the passage of finite-amplitude interfacial waves is governed by Laplace's equations (2.72). We seek solutions in the x–z plane that are horizontally periodic with wavenumber k and which are bounded as $z \to \pm\infty$. Although the partial differential equations are linear, finite amplitude effects are captured by the nonlinear interface conditions (2.73) and (2.74), here with ϕ_1 replaced by φ and ϕ_2 replaced by ϕ.

Isolating η in the first of these conditions gives

$$g(\rho_2 - rho_1)\eta = \left[\rho_1\left(\frac{\partial\varphi}{\partial t} + \frac{1}{2}|\nabla\varphi|^2\right) - \rho_2\left(\frac{\partial\phi}{\partial t} + \frac{1}{2}|\nabla\phi|^2\right)\right]\Bigg|_{z=\eta}. \tag{4.38}$$

The remaining interface condition gives two equations:

$$\left.\frac{\partial\varphi}{\partial z}\right|_{z=\eta} = \left.\frac{\partial\phi}{\partial z}\right|_{z=\eta} \tag{4.39}$$

and

$$\left.\frac{\partial\phi}{\partial z}\right|_{z=\eta} = \left(\frac{\partial}{\partial t} + \nabla\phi\cdot\nabla\right)\eta\Bigg|_{z=\eta}. \tag{4.40}$$

Another condition could be posed by replacing ϕ with φ in (4.40), but this adds no new information.

Assuming that η is small but not negligibly so, we perform a Taylor-series expansion about $\eta = 0$ for each of the interface conditions (4.38), (4.39) and (4.40). Generally, for a function $f(x,z,t)$ which is smooth near $z = 0$ we can write

$$f|_{z=\eta} \simeq f|_{z=0} + \eta\left.\frac{\partial f}{\partial z}\right|_{z=0} + \frac{1}{2}\eta^2\left.\frac{\partial^2 f}{\partial z^2}\right|_{z=0} + \ldots \tag{4.41}$$

In particular,

$$\phi(x,\eta,t) \simeq \phi(x,0,t) + \eta\,\phi_z(x,0,t) + \ldots \tag{4.42}$$

Following the methodology described in Section 4.2.2, we now use perturbation theory for differential eigenvalue problems to determine how the structure and

frequency of the waves vary with amplitude. We expand η, φ, ϕ and the squared frequency ω^2 as power series in A_0 using (4.13) so that

$$\begin{aligned}
\eta &= A_0\left(\eta_0 + A_0\eta_1 + {A_0}^2\eta_2 + \ldots,\right),\\
\varphi &= A_0\left(\varphi_0 + A_0\varphi_1 + {A_0}^2\varphi_2 + \ldots,\right),\\
\phi &= A_0\left(\phi_0 + A_0\phi_1 + {A_0}^2\phi_2 + \ldots,\right),\\
\omega^2 &= {\omega_0}^2\left(1 + {A_0}^2\sigma_2 + \ldots\right).
\end{aligned} \tag{4.43}$$

Arbitrarily, we can treat A_0 as the vertical displacement amplitude. Though it would be more rigorous to use the nondimensional amplitude $\alpha = kA_0$ as our perturbation parameter, it is sufficient here to use A_0 and then extract terms in successive powers of A_0, as done in Section 4.2.2. The functions η_i, φ_i and ϕ_i are defined to be independent of A_0 so that these functions and their derivatives are of order unity.

Substituting the expansions for φ and ϕ into Laplace's equation for the upper and lower layers and extracting terms at successive powers of A_0 gives the sequence of partial differential equations $\nabla^2\varphi_i = 0$ and $\nabla^2\phi_i = 0$. The subscript $i = 0, 1, 2, \ldots$ corresponds to successive orders in the perturbation expansion.

At leading order, for which terms are of order A_0, we seek horizontally periodic, vertically bounded solutions of $\nabla^2\varphi_0 = 0$ and $\nabla^2\phi_0 = 0$, subject to the leading-order terms of the interface conditions (4.38), (4.39) and (4.40). Eliminating η_0 from these gives a matrix operator equation in φ_0 and ϕ_0 alone:

$$L_0\vec{\phi}_0\Big|_{z=0} = 0, \tag{4.44}$$

in which

$$L_0 \equiv \begin{pmatrix} \partial_z & -\partial_z \\ {\rho_1\omega_0}^2 & \rho_2(g'\partial_z - {\omega_0}^2) \end{pmatrix} \text{ and } \vec{\phi}_0 \equiv \begin{pmatrix} \varphi_0 \\ \phi_0 \end{pmatrix}. \tag{4.45}$$

The first row comes from (4.39) after expanding φ and ϕ using (4.41). The second row comes from combining the linearized forms of (4.38) and (4.40) to eliminate η. The second time derivatives in the result are replaced with $-\omega^2$ and this is expanded using the last expression in (4.43).

From (4.38), the leading-order equation defining the vertical displacement in terms of $\vec{\phi}_0$ is

$$\eta_0 = -\frac{1}{\rho_2 g'}\left[\rho_1\frac{\partial\varphi_0}{\partial t} - \rho_2\frac{\partial\phi_0}{\partial t}\right]\Bigg|_{z=0}. \tag{4.46}$$

Just as we found in Section 2.3, the eigensolutions for small-amplitude interfacial waves are given by

$$\begin{aligned}\eta_0 &= \cos(kx-\omega t)\\ \varphi_0 &= -\frac{\omega}{k}e^{-kz}\sin(kx-\omega t),\ \ z>0\\ \phi_0 &= \frac{\omega}{k}e^{kz}\sin(kx-\omega t),\ \ z<0,\end{aligned} \tag{4.47}$$

in which

$$\omega^2 = {\omega_0}^2 = \frac{\rho_2-\rho_1}{\rho_1+\rho_2}gk. \tag{4.48}$$

Here the structure of the waves is represented by the actual values rather than as complex exponentials and the phase has been chosen so that $\eta = A_0\eta_0$ has its maximum value A_0 at $x = t = 0$.

At the next highest order the interface conditions can be written

$$L_0\vec{\phi}_1\Big|_{z=0} = \vec{N}_1(\varphi_0,\phi_0,\eta_0)\Big|_{z=0}, \tag{4.49}$$

in which L_0 is defined as in (4.45) and the forcing due to quadratic interactions between the leading-order fields is given by

$$\vec{N}_1 = \begin{pmatrix} -\eta_0\partial_z[\partial_z\varphi_0-\partial_z\phi_0] \\ -\eta_0\partial_z[\rho_1{\omega_0}^2\varphi_0+\rho_2(g'\partial_z-{\omega_0}^2)\phi_0]+ \\ \rho_1\nabla\varphi_0\cdot\nabla\varphi_{0t}-\rho_2\nabla\phi_0\cdot\nabla\phi_{0t}+\rho_2 g'\nabla\phi_0\cdot\nabla\eta_0 \end{pmatrix}. \tag{4.50}$$

From (4.44) and (4.45), it follows immediately that both terms within square brackets in (4.50) are zero. Furthermore, with substitution of the leading-order solutions of (4.48) into the remaining nonlinear terms in (4.50), we find that both expressions in the vector are identically zero. Therefore, $\vec{\phi}_1$ is independent of $\vec{\phi}_0$, and so we set

$$\varphi_1 = \phi_1 = 0. \tag{4.51}$$

However, η_1 is not independent of $\vec{\phi}_0$. At this order of A_0, the power series expansion of (4.38) gives

$$\rho_2 g'\eta_1 = \left[\rho_1\left(\eta_0\partial_{zt}\varphi_0+\frac{1}{2}|\nabla\varphi_0|^2\right)-\rho_2\left(\eta_0\partial_{zt}\phi_0+\frac{1}{2}|\nabla\phi_0|^2\right)\right]\Bigg|_{z=0}.$$

Using (4.47), we find

$$\eta_1 = \frac{1}{2}k\,\frac{\rho_2-\rho_1}{\rho_1+\rho_2}\cos 2(kx-\omega t). \tag{4.52}$$

The next order in the perturbation expansion introduces the order ${A_0}^2$ correction to the squared frequency. Thus, by analogy with (4.20), the interface conditions are written

$$\left[L_0\vec{\phi}_2 + L_2\vec{\phi}_0\right]\Big|_{z=0} = \vec{N}_2(\varphi_0, \phi_0, \eta_0, \eta_1)\Big|_{z=0}, \tag{4.53}$$

in which

$$L_2(\sigma_2) \equiv \begin{pmatrix} 0 & 0 \\ \rho_1{\omega_0}^2\sigma_2 & -\rho_2{\omega_0}^2\sigma_2 \end{pmatrix}. \tag{4.54}$$

The nonlinear terms in $\vec{N}_2$ are either cubic in the leading-order terms or involve products of η_1 with the leading-order terms. As in the simplification of (4.50), some of the terms can immediately be set to zero. After extensive algebra the remaining terms can be written as a superposition of functions involving $\sin(kx-\omega t)$, $\cos(kx-\omega t)$, $\sin 3(kx-\omega t)$ and $\cos 3(kx-\omega t)$.

The terms proportional to $\sin(kx-\omega t)$ and $\cos(kx-\omega t)$ are resonant with the linear term $L_0\phi_2$ and would result in the unphysical growth of the waves over time. But these secular terms can be eliminated with the appropriate choice of σ_2. Explicitly, we find the correct choice that gets rid of the secular terms is

$$\sigma_2 = \frac{{\rho_1}^2 + {\rho_2}^2}{(\rho_1+\rho_2)^2}{A_0}^2k^2. \tag{4.55}$$

Therefore, to this order accuracy the dispersion relation is

$$\omega^2 = gk\frac{\rho_2-\rho_1}{\rho_2+\rho_1}\left(1 + \frac{{\rho_1}^2+{\rho_2}^2}{(\rho_1+\rho_2)^2}{A_0}^2k^2\right). \tag{4.56}$$

We next compute the correction to φ, ϕ and η at this order. In particular, together with (4.47) and (4.52), the interfacial displacement accurate to amplitude-cubed is

$$\begin{aligned}\eta = {} & A_0\cos(kx-\omega t) + \frac{1}{2}{A_0}^2k\frac{\rho_2-\rho_1}{\rho_1+\rho_2}\cos 2(kx-\omega t) \\ & + \frac{3}{8}{A_0}^3k^2\left(\frac{(\rho_2-\rho_1)^2 - 4\rho_1\rho_2/3}{(\rho_1+\rho_2)^2}\right)\cos 3(kx-\omega t).\end{aligned} \tag{4.57}$$

The following sections examine the structure and dispersion of weakly nonlinear interfacial waves in the limit of deep surface waves and of Boussinesq interfacial waves.

4.3.2 Deep water waves

Because the density of air is much less than that of water, the dispersion relation and structure of deep water waves is found by taking the limit $\rho_1 \to 0$ in (4.56) and

(4.57), respectively. Explicitly, their dispersion relation is given by

$$\omega^2 = gk\left(1 + {A_0}^2 k^2\right). \tag{4.58}$$

As for small-amplitude waves, it is understood that $k > 0$ in (4.58) and that the directionality of the waves is set by the sign of ω. Without loss of generality, we assume $\omega > 0$ corresponding to rightward-propagating waves. Explicitly, $\omega \simeq \sqrt{gk}\left(1 + {A_0}^2 k^2/2\right)$.

If $A_0 k \ll 1$, (4.58) reduces to the dispersion relation of small-amplitude deep water waves as given by (2.18). The frequency and phase speed of the waves increases with amplitude. The group velocity is modified according to (4.35) in which $\omega_0 = (gk)^{1/2}$ and $\omega_2 = (gk^5)^{1/2}/2$. But computing the term inside the square root on the right-hand side of (4.35), we find

$$\omega_2 {\omega_0}'' = -\frac{1}{8} gk. \tag{4.59}$$

Because k is strictly positive this expression is always negative. Therefore deep water waves of all wavenumbers are modulationally unstable. Even infinitesimally small-amplitude wavepackets will initially grow in amplitude, though at a very small growth rate compared to the frequency.

Taking the first two terms in (4.57), the surface displacement of moderately large-amplitude deep surface waves is

$$\eta \simeq A_0 \left[\cos(kx - \omega t) + \frac{1}{2} A_0 k \cos 2(kx - \omega t)\right]. \tag{4.60}$$

At crests the two terms superimpose to increase the surface displacement. Conversely, at troughs they superimpose so that the downward displacement is not so great. That is, finite-amplitude effects act to flatten the troughs and sharpen the crests, as illustrated in Figure 4.2. The top two graphs show the structure of waves with small and moderately large amplitude.

As the amplitude A_0 becomes larger, it is necessary to compute increasingly higher-order terms in the Fourier cosine series representation for A_0. The amplitude is limited, however. As first shown by Stokes, at a critical value of A_0 the wave crests develop sharp peaks which form an angle of 120° across the cusp, as shown in Figure 4.2c (see Exercises). The crest-to-trough distance in this case is approximately $0.44 k^{-1} \simeq 0.071\lambda$. For still larger-amplitude waves, the crest spills and the wave breaks.

In idealized circumstances, the weakly nonlinear structure of a train of deep water waves is also modified through development of periodic cusping along the span of the waves. Such dynamics have been neglected here but are discussed in references cited in Appendix A.

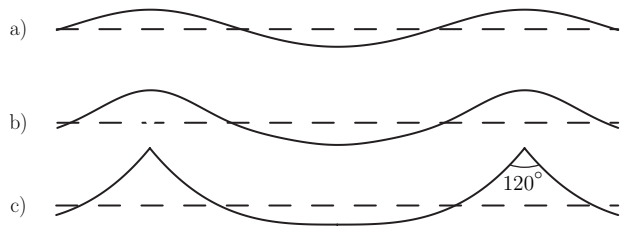

Fig. 4.2. Comparison of the surface displacement structure of a deep water wave whose amplitude is a) small b) moderate and c) at the point of breaking. The structure of the small- and moderate-amplitude waves is given by (4.60). The large-amplitude wave has a crest-to-trough distance of $0.44k^{-1} \simeq 0.071\lambda$ and the cusps at their crests form a 120° angle. Note, the aspect ratios of the plots are not to scale.

4.3.3 Deep interfacial plane waves

We now consider the motion of the interface between two fluids of comparable density for which the upper and lower layers are infinitely deep. Taking the Boussinesq limit $\rho_1 \to \rho_2{}^-$ in (4.56), the dispersion relation becomes

$$\omega^2 \simeq \frac{1}{2}g'k\left(1+\frac{1}{2}{A_0}^2k^2\right), \tag{4.61}$$

in which the reduced gravity g' is given by

$$g' \equiv g\frac{\rho_2-\rho_1}{\rho_2}. \tag{4.62}$$

As for deep water waves, finite-amplitude effects act to increase their frequency and phase speed, and the group velocity (4.35) is modified by an imaginary term proportional to amplitude, meaning that the waves are modulationally unstable.

The structure of the waves is not purely sinusoidal when they grow to large amplitude. Taking the Boussinesq limit of (4.57), the surface displacement is

$$\eta = A_0\left[\cos(kx-\omega t) - \tfrac{1}{8}{A_0}^2k^2\cos 3(kx-\omega t)\right]. \tag{4.63}$$

Note that the order ${A_0}^2$ term vanishes in the Boussinesq limit so that, unlike the formula (4.60) for deep water waves, the leading-order finite-amplitude correction to the small-amplitude wave structure is of order ${A_0}^3$. This has a number of interesting implications.

First, there is no bias for the waves to have sharp crests and shallow troughs, as was the case for deep water waves. Instead, both the crests and troughs of finite-amplitude interfacial Boussinesq waves are flatter than their small-amplitude sinusoidal counterparts, as shown in Figure 4.3. This symmetry is anticipated

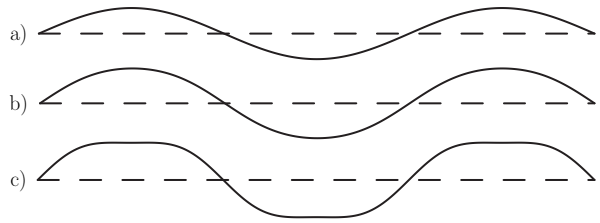

Fig. 4.3. Comparison of the structure of interfacial Boussinesq waves at a) small, b) moderate and c) large amplitude.

because in the Boussinesq approximation the equations of motion are invariant upon reflection in z.

On the other hand, because the finite-amplitude correction is of order ${A_0}^3$, in comparison with deep surface waves interfacial waves would have to get to quite large amplitude before the flattening of crests and troughs becomes evident. In reality, they are unlikely to occur to any significant degree because of other dynamics that occur at finite amplitude. In Section 2.3.2 we found that the fluid moves leftwards above and rightwards below the interface of a rightward-advancing wave crest. Thus the mechanism for interfacial wave breaking is different than that for deep surface waves: their amplitude is limited not by the development of cusped peaks but by the development of small-scale shear instabilities as discussed, for example, in Section 2.6.3.

4.3.4 Deep interfacial wavepackets

The evolution of the amplitude envelope $A(x,t)$ of a quasi-monochromatic wavepacket whose wavenumber spectrum is peaked about $k = k_0$ is given by (4.27). Using (4.61), the equation for the interfacial displacement is given explicitly by

$$\imath\,(A_t - c_g A_x) = \frac{1}{4}\omega_0(k_0)\left[+\frac{1}{2}{k_0}^{-2}A_{xx} + {k_0}^2|A|^2A\right], \tag{4.64}$$

in which x- and t-subscripts denote space and time derivatives, $\omega_0(k_0) = (g'k_0/2)^{1/2}$, and the group velocity of small-amplitude waves is $c_g = (g'/8k_0)^{1/2} = \frac{1}{2}\omega_0/k_0$.

Equation (4.64) has been written in a way that is straightforwardly converted into nondimensional form. Defining $\tilde{T} = \omega_0 t$, $\tilde{X} = k_0\,(x - c_g t)$ and $\tilde{A} = k_0 A$ gives the nonlinear Schrödinger equation

$$\imath\tilde{A}_{\tilde{T}} = \frac{1}{8}\tilde{A}_{\tilde{X}\tilde{X}} + \frac{1}{4}|\tilde{A}|^2\tilde{A}. \tag{4.65}$$

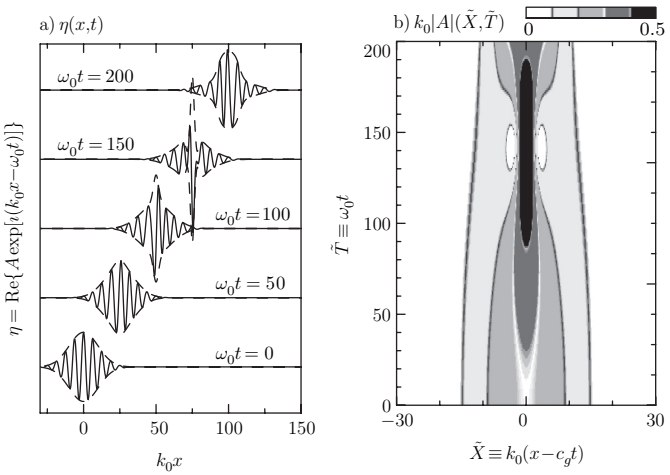

Fig. 4.4. Weakly nonlinear evolution of a Gaussian interfacial wavepacket prescribed initially with amplitude $A_0 k_0 = 0.3$ and width $\sigma k_0 = 10$. The solid lines in a) show a vertically shifted sequence of graphs of the vertical displacement field, η (solid line) with the amplitude envelope, $|A|$ (dashed line), at the times indicated. The time series of the amplitude envelope $|A|$ are shown by the greyscale contours in b). This is plotted in a frame of reference moving with the wavepacket.

Note that the advection term $c_g A_x$ on the left-hand side of (4.64) has disappeared as a consequence of defining $\tilde{X}$ to be a spatial co-ordinate in the frame of reference moving with the wavepacket at the group velocity.

Figure 4.4 shows the predicted evolution of a weakly nonlinear deep interfacial wavepacket whose vertical displacement field is given initially by

$$\eta = A_0 e^{-x^2/2\sigma^2} \cos(k_0 x - \omega_0 t).$$

Solving (4.64) in the case with $A_0 k_0 = 0.3$ and $\sigma k_0 = 10$ shows that the wavepacket narrows and its maximum amplitude more than doubles at times around $t \simeq 150{\omega_0}^{-1}$. Thereafter the wavepacket broadens and the peak amplitude decreases again.

The growth in amplitude is the result of modulational instability and the narrowing then broadening of the wavepacket is an example of the Fermi–Pasta–Ulam recurrence phenomenon.

4.3.5 Interfacial waves in finite-depth fluid

Up until now we have ignored the presence of solid horizontal boundaries situated above or below the interface. Although the mathematical method to determine the weakly nonlinear behaviour of finite-depth interfacial waves is the same as

that above, the algebra is more cumbersome and only the salient results will be given here.

We first consider a two-layer Boussinesq fluid with an unbounded upper layer and a lower layer bounded below by a rigid horizontal boundary at depth H below the mean-depth of the interface. This circumstance might crudely model an atmospheric inversion in the absence of a mean wind. By symmetry, the result can be flipped vertically to describe waves at an interface beneath a finite-depth upper layer. This might describe a model thermocline in the ocean or a lake, for which the surface can be treated as rigid.

The dispersion relation in both circumstances is the same:

$$\omega^2 \simeq g'k \,\frac{1}{\coth kH + 1} \times \left[1 + \frac{9 - 22\tanh kH + 13\tanh^2 kH + 4\tanh^3 kH}{8\tanh kH} (A_0 k)^2 \right]. \tag{4.66}$$

As expected, in the limit $H \to \infty$, this reduces to the dispersion relation (4.61) for interfacial waves in infinitely deep fluid.

The polynomial in $\tanh kH$ in the numerator of the fraction in (4.66) is always positive. As a consequence these waves, like those discussed above, are modulationally unstable for all k.

At second order in amplitude, the weakly nonlinear structure of the waves above a finite-depth lower layer is

$$\eta = A_0 \left[\cos(kx - \omega t) + \frac{3}{4} \frac{1 - \tanh kH}{\tanh^2 kH} (A_0 k) \cos 2(kx - \omega t) \right]. \tag{4.67}$$

Unlike the case of interfacial waves in infinite-depth fluid, but similar to the weakly nonlinear behaviour of surface waves, here we find the wave crests sharpen and the troughs flatten as a consequence of finite-amplitude effects. Specifically, the waves form peaks in the direction oriented towards the deeper fluid, as shown in Figure 4.5.

A second class of weakly nonlinear waves exists in semi-infinite fluids in the near-shallow water limit. These are solitary waves. Because the development and solution of these equations are distinct from those discussed in this section, we defer discussion of solitary waves to Section 4.4.

Beforehand we consider the special case of a finite-depth Boussinesq fluid in which the upper- and lower-layer fluids have approximately the same depth, $H_1 \simeq H_2 \equiv H$. Though geophysically irrelevant, it is a symmetric geometry that has been singled out for study in laboratory experiments.

As in the case of interfacial waves in a two-layer fluid that is unbounded above and below, we find the interfacial waves in a bounded, equal-depth, two-layer fluid

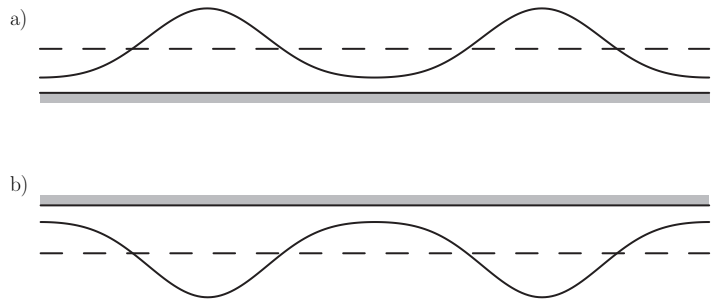

Fig. 4.5. The structure of weakly nonlinear interfacial waves in a fluid with a) a shallow lower layer and b) a shallow upper layer.

do not form cusps but flatten with respect to the sinusoidal structure of small-amplitude waves at both the crests and troughs. For long waves, an expansion in the form (4.13) is possible provided $[(A_0k)/(kH)^2]^2$ is small. In this case, the dispersion relation is

$$\omega^2 \simeq \frac{1}{2}g'k\left[1+\left(1-\frac{1}{2}\coth^2 kH\right)(A_0k)^2\right]. \tag{4.68}$$

If the amplitude is sufficiently large, the structure of interfacial waves in finite-depth fluid depends sensitively upon the departure from symmetry. The crests and troughs are smooth if $(H_2/H_1)^2 < \rho_2/\rho_1$ and they form downward cusps if $(H_2/H_1)^2 > \rho_2/\rho_1$. The transition occurs when the lower layer is deeper than the upper layer by an amount $H_1(\Delta\rho/\rho_1)/2$.

4.4 Solitary waves

Originally, solitary waves referred to finite-amplitude and isolated (hence solitary) disturbances of permanent form. In fluid dynamics these are hump-shaped waves which, for example, have a crest but no trough. The waves exist in finite-depth fluid which typically has one or two layers and the horizontal extent of the wave is long, but not too long, compared with the depth of the fluid.

Despite being large-amplitude, the waves maintain their structure through a balance between dispersion, which tends to broaden the crest, and weakly nonlinear effects, which tend to steepen it. Whereas fluid beneath a small-amplitude shallow water wave oscillates back and forth but experiences no net displacement, fluid beneath a solitary wave is permanently displaced a finite distance which is comparable to the horizontal extent of the wave, as required by continuity of mass. This is shown in Figure 4.6.